STRUCTURAL BIOLOGY COMMUNICATIONS

ISSN 2053-230X

High-resolution crystal structure of the reduced Grx1 from *Saccharomyces cerevisiae*

Shadi Maghool,[a]* Sharon La Fontaine[b] and Megan J. Maher[a]*

[a]Department of Biochemistry and Genetics, La Trobe Institute for Molecular Science, La Trobe University, Melbourne, Victoria, Australia, and [b]School of Life and Environmental Sciences, Deakin University, Melbourne, Victoria, Australia. *Correspondence e-mail: s.maghool@latrobe.edu.au, m.maher@latrobe.edu.au

Received 18 November 2018
Accepted 7 March 2019

Edited by M. J. Romao, Universidade Nova de Lisboa, Portugal

Keywords: glutaredoxin; *Saccharomyces cerevisiae*; Grx1; reduced form.

PDB reference: reduced Grx1, 6mws

Supporting information: this article has supporting information at journals.iucr.org/f

Grx1, a cytosolic thiol–disulfide oxidoreductase, actively maintains cellular redox homeostasis using glutathione substrates (reduced, GSH, and oxidized, GSSG). Here, the crystallization of reduced Grx1 from the yeast *Saccharomyces cerevisiae* (yGrx1) in space group $P2_12_12_1$ and its structure solution and refinement to 1.22 Å resolution are reported. To study the structure–function relationship of yeast Grx1, the crystal structure of reduced yGrx1 was compared with the existing structures of the oxidized and glutathionylated forms. These comparisons revealed structural differences in the conformations of residues neighbouring the Cys27–Cys30 active site which accompany alterations in the redox status of the protein.

1. Introduction

Glutaredoxins (Grxs) are intracellular GSH-dependent oxidoreductase enzymes (EC 1.8.1.7). They catalyze reversible thiol–disulfide exchange reactions between protein thiols and GSSG/GSH and hence play a critical role in the maintenance of cellular redox homeostasis (Holmgren, 1989; Prinz *et al.*, 1997). Glutaredoxin enzymes act to protect cells from damage caused by reactive oxygen species (ROS) by catalyzing the reduction of protein disulfides (P-SS) and the deglutathionylation of mixed disulfides (P-SSG), and the overall direction of the reactions depend on the reduction potential of the GSSG/2GSH couple, the nature of the protein thiols involved and other solution conditions such as the presence of metal ions. In the reduction of glutathionylated disulfides (deglutathionylation reaction mechanism), the N-terminal active-site cysteine of Grx exists as a thiolate anion and attacks the glutathionyl sulfur of the P-SSG mixed disulfide, forming a Grx enzyme intermediate [Grx(SH)(SSG)] and releasing the reduced protein (P-SH). The Grx mixed disulfide is reduced by GSH, forming oxidized GSSG, which is then reduced to GSH by glutathione reductase and NADPH (Begas *et al.*, 2017; Ukuwela *et al.*, 2017, 2018). Structurally, Grxs share a common structural fold with the thioredoxin (TRX) superfamily, which is represented by a central core of four β-strands surrounded by five α-helices and an active-site C*XX*C sequence motif (Martin, 1995; Cave *et al.*, 2001).

Five Grxs have been characterized from the yeast *S. cerevisiae* to date. These include Grx1 (yGrx1) and Grx2, which contain an active-site CPYC (Luikenhuis *et al.*, 1998) motif which participates in redox processes through the formation of a disulfide bond between the two cysteine residues or *via* glutathionylation of the first cysteine residue (Holmgren, 1989; Prinz *et al.*, 1997; Ritz & Beckwith, 2001). However,

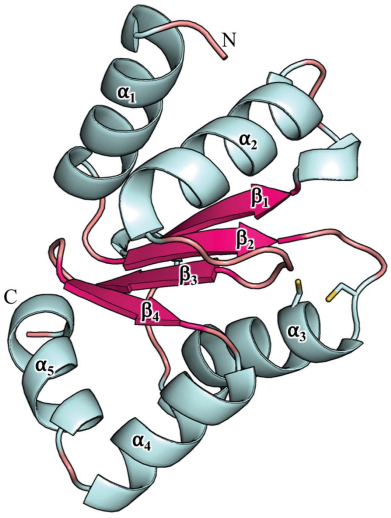

Table 1
Macromolecule-production information.

Source organism	*S. cerevisiae*
DNA source	*S. cerevisiae*
Expression vector	pGEX-6p-1
Expression host	*E. coli* strain BL21 CodonPlus (DE3)
Complete amino-acid sequence of the construct	GPLGSMVSQETIKHVKDLIAENEIFVASKT YCPYCHAALNTLFEKLKVPRSKVLVLQL NDMKEGADIQAALYEINGQRTVPNIYIN GKHIGGNDDLQELRETGELEELLEPILA N

other Grxs (Grx3, Grx4 and Grx5) from this organism contain only a single cysteine residue in an active-site CGFS motif, which catalyses the (de)glutathionylation of protein thiol groups using glutathione substrates (reduced, GSH, and oxidized, GSSG; Rodríguez-Manzaneque *et al.*, 1999). Crystal structures of the yGrx1 enzyme in the oxidized, glutathionylated (Yu *et al.*, 2008) and glutathionylated C30S mutant (Håkansson & Winther, 2007) forms have been reported previously (PDB entries 3c1r, 3c1s and 2jac, respectively). Here, we augment these structures with the first structure of yGrx1 in the reduced form in the absence of glutathionylation. A comparison of the structure of reduced yGrx1 (^{red}yGrx1; PDB entry 6mws, this work) with the structures of the oxidized (^{ox}yGrx1; PDB entry 3c1r) and glutathionylated (^{glu}yGrx1; PDB entry 3c1s) forms reveals conformational changes which accompany alterations in the redox status of this protein.

2. Materials and methods

2.1. Macromolecule production

The pGEX-6p-1-yGrx1 (GenScript) plasmid was transformed into *Escherichia coli* strain BL21 CodonPlus (DE3). Cultures were grown at 310 K in Luria Broth (LB) supplemented with ampicillin (100 µg ml^{-1}) and chloramphenicol (35 µg ml^{-1}) to an OD_{600} of 0.8, induced with isopropyl β-D-1-thiogalactopyranoside (IPTG; 0.5 m*M*) and harvested after 16 h (with shaking) at 298 K.

GST-yGrx1 was purified by GSH affinity chromatography. Frozen cell pellets were thawed at room temperature and resuspended in cell-lysis buffer [phosphate-buffered saline (PBS) pH 7.4, 1 m*M* tris(2-carboxyethyl)phosphine hydrochloride (TCEP)]. The cells were disrupted by passage through a TS series bench-top cell disruptor (Constant Systems) at 241 MPa. Cell debris was removed by centrifugation (Beckman JLA-25.50, 30 000*g*, 20 min, 277 K) and the soluble fraction was incubated for 2 h at 277 K with glutathione Sepharose 4B resin (GE Healthcare) equilibrated with lysis buffer (PBS containing 1 m*M* TCEP). The GST tag was cleaved overnight in lysis buffer with PreScission Protease followed by size-exclusion chromatography (SEC; HiLoad 16/600 Superdex 75 pg, GE Healthcare; 20 m*M* Tris–MES pH 8.0, 150 m*M* NaCl, 1 m*M* TCEP). Cleavage of the N-terminal GST tag introduced five additional residues (GPLGS) to the N-terminus of yGrx1 (Table 1). The purified protein was concentrated to 20 mg ml^{-1} before storage at 193 K.

Table 2
Crystallization.

Method	Hanging-drop vapour diffusion
Plate type	VDXm plates
Temperature (K)	293
Protein concentration (mg ml^{-1})	16
Buffer composition of protein solution	20 m*M* Tris–MES pH 8.0, 150 m*M* NaCl, 1 m*M* TCEP
Composition of reservoir solution	0.23 *M* lithium sulfate monohydrate, 0.1 *M* bis-Tris pH 5.8, 26%(*w*/*v*) PEG 3350
Volume and ratio of drop	2 µl, 1:1
Volume of reservoir (µl)	500

2.2. Crystallization

Crystallization trials were conducted using commercially available screens (SaltRx HT and Index HT from Hampton Research) by sitting-drop vapour diffusion in 96-well plates (Molecular Dimensions) using pure yGrx1 samples at two different protein concentrations (10 and 20 mg ml^{-1}). Crystallization drops consisting of equal volumes (0.2 µl) of reservoir and protein solutions were dispensed using a Crystal Gryphon liquid-handling system (Art Robbins Instruments) and were equilibrated against a reservoir of screen solution (50 µl). Plates were incubated at 293 K. Multiple tiny crystals were observed within ten days in conditions F7 and G2 of the Index HT screen [0.2 *M* ammonium sulfate, 0.1 *M* bis-Tris pH 6.5, 25%(*w*/*v*) PEG 3350 and 0.2 *M* lithium sulfate monohydrate, 0.1 *M* bis-Tris pH 5.5, 25%(*w*/*v*) PEG 3350, respectively]. Optimization of these conditions was carried out by hanging-drop vapour diffusion in 24-well VDX plates (Hampton Research). Diffraction-quality crystals of yGrx1 grew after 20 days in drops consisting of equal volumes (1 µl) of yGrx1 (16 mg ml^{-1} in 20 m*M* Tris–MES pH 8.0, 150 m*M* NaCl, 1 m*M* TCEP) and reservoir [0.23 *M* lithium sulfate monohydrate, 0.1 *M* bis-Tris pH 5.8, 26%(*w*/*v*) PEG 3350] solutions equilibrated against 500 µl reservoir solution. Crystals were cryoprotected in reservoir solution containing 25%(*w*/*v*) glycerol before flash-cooling them in liquid nitrogen. Crystallization information is summarized in Table 2.

2.3. Data collection and processing

Diffraction data were recorded on beamline MX2 at the Australian Synchrotron at a wavelength of 0.954 Å at 100 K using an EIGER X 16M detector and were processed with *XDS* (Kabsch, 2010) and merged and scaled with *AIMLESS* (Evans & Murshudov, 2013). Data-collection statistics are detailed in Table 3.

2.4. Structure solution and refinement

The crystal structure of yGrx1 was solved by molecular replacement using *Phaser* (McCoy *et al.*, 2007) from the *CCP*4 suite (Winn *et al.*, 2011). The crystal structure of oxidized yGrx1 (Yu *et al.*, 2008) was used as a search model after the removal of all water molecules. The model was refined using *REFMAC*5 (Murshudov *et al.*, 2011) and manual model building was carried out in *Coot* (Emsley *et al.*, 2010). Automated water picking was carried out using *ARP*/*wARP* (Langer *et al.*, 2008) and was then checked manually in *Coot*

Table 3
Data collection and processing.

Values in parentheses are for the outer shell.

Diffraction source	MX2, Australian Synchrotron
Wavelength (Å)	0.953654
Temperature (K)	100
Detector	EIGER X 16M
Crystal-to-detector distance (mm)	150
Total rotation range (°)	180
Space group	$P2_12_12_1$
a, b, c (Å)	41.4, 51.8, 57.2
α, β, γ (°)	90.0, 90.0, 90.0
Mosaicity (°)	0.04
Resolution range (Å)	41.36–1.22 (1.25–1.22)
Total No. of reflections	474455 (17110)
No. of unique reflections	37323 (1777)
Completeness (%)	99.9 (98.3)
Multiplicity	12.7 (9.6)
$\langle I/\sigma(I)\rangle$	19.4 (4.0)
$CC_{1/2}$	0.999 (0.969)
R_{merge}	0.053 (0.319)
Overall B factor from Wilson plot (Å^2)	14.2

Table 4
Structure solution and refinement.

Values in parentheses are for the outer shell.

Resolution range (Å)	38.38–1.22 (1.25–1.22)
Completeness (%)	99.9 (98.3)
σ Cutoff	None
No. of reflections, working set	35443
No. of reflections, test set	1820
Final R_{cryst}	0.148 (0.149)
Final R_{free}	0.171 (0.159)
No. of non-H atoms	
Protein	854
Sulfate	5
Water	122
Total	981
R.m.s. deviations	
Bonds (Å)	0.010
Angles (°)	1.430
Average B factors (Å^2)	
Protein	13.731
Sulfate	14.822
Water	23.273
Ramachandran plot	
Most favoured (%)	99.1
Allowed (%)	100
MolProbity score	0.82
PDB code	6mws

(Emsley *et al.*, 2010). The quality of the structure was determined by *MolProbity* (Chen *et al.*, 2010). Refinement statistics are summarized in Table 4.

3. Results and discussion

The ^{red}yGrx1 crystallized in space group $P2_12_12_1$, with unit-cell parameters a = 41.4, b = 51.8, c = 57.2 Å. The structure was determined by molecular replacement and refined to 1.22 Å resolution. The refinement converged with residuals R_{cryst} = 14.8% and R_{free} = 17.1%. The solvent content of the crystal was 60% and the structure shows a single molecule of ^{red}yGrx1 (residues Val2–Ala109) in the asymmetric unit. Owing to an absence of interpretable electron density for the five additional N-terminal residues (GPLGS) and the N-terminal and C-terminal residues of yGrx1 (Met1 and

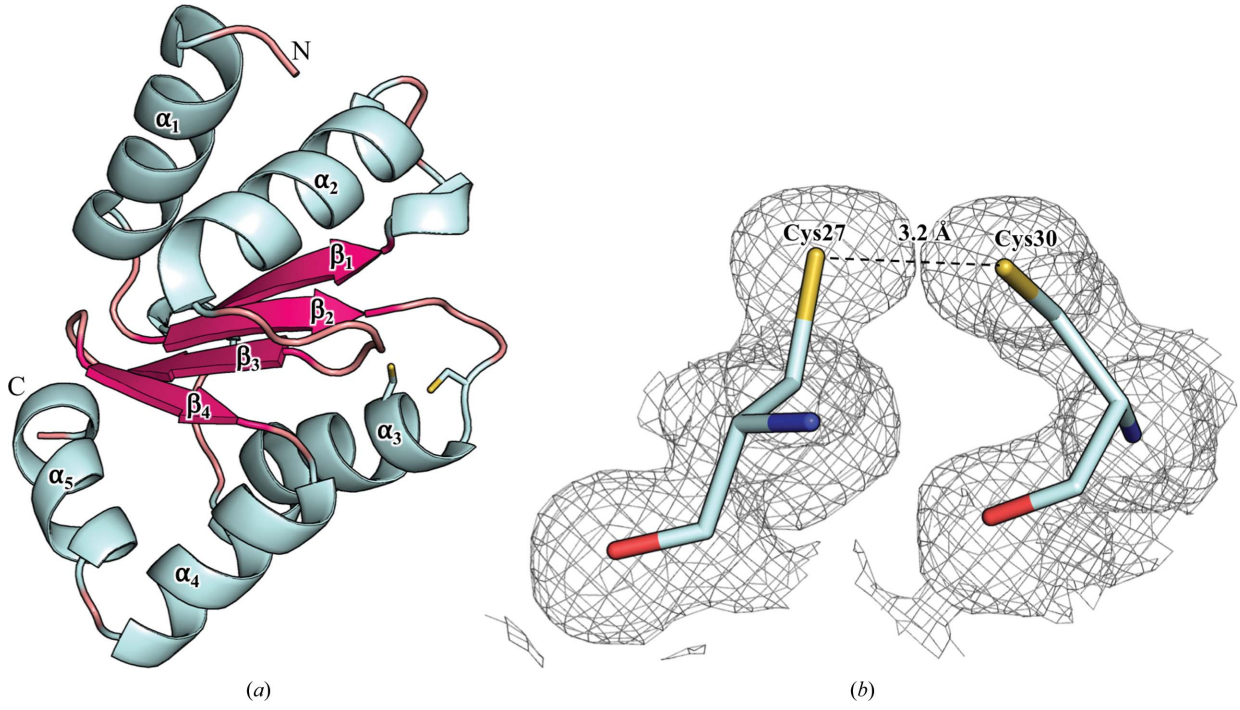

Figure 1
Cartoon representation of the overall structure of ^{red}yGrx1. (*a*) Secondary structures are represented as cartoons, with α-helices and β-strands coloured cyan and pink, respectively. The Cys27 and Cys30 residues are shown as yellow sticks. (*b*) $F_o - F_c$ difference Fourier electron-density map calculated after omission of the Cys27 and Cys30 residues from the model coordinates. C, O, N and S atoms are coloured cyan, red, blue and yellow, respectively. The $F_o - F_c$ map is contoured at 4σ.

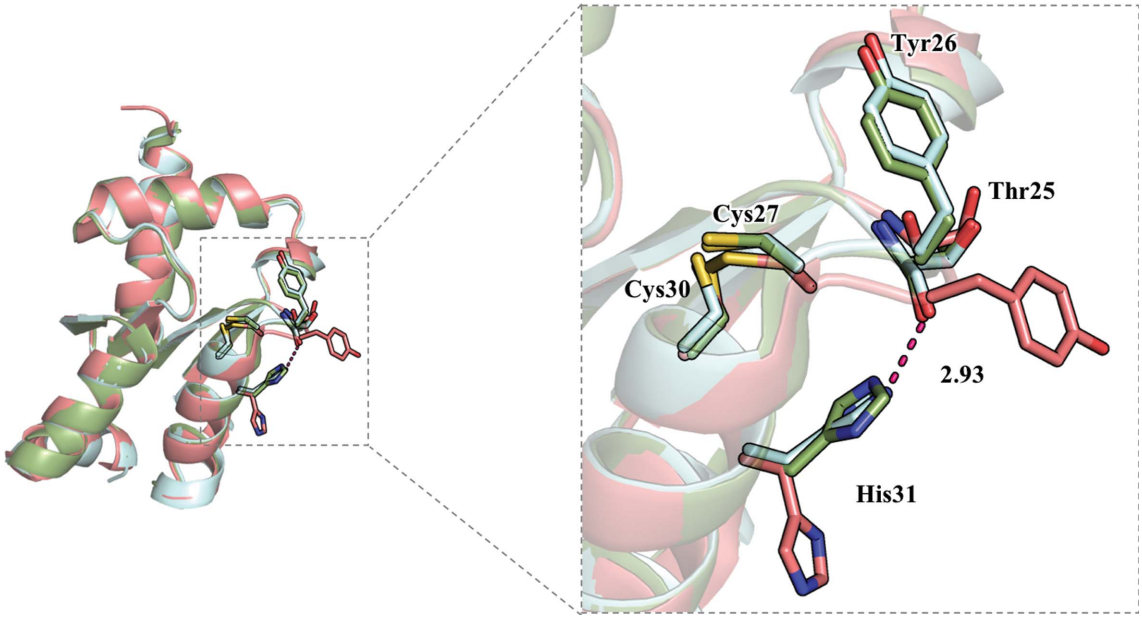

Figure 2
Details of the yGrx1 active site (CPYC) upon reduction (cyan), oxidization (salmon) and glutathionylation (green). Comparison of the ^{red}yGrx1 (cyan), ^{ox}yGrx1 (PDB entry 3c1r; salmon) and ^{glu}yGrx1 (PDB entry 3c1s; green) structures shows that upon the separation of the Cys27 and Cys30 residues owing to reduction or glutathionylation, the Thr25, Tyr26 and His31 residues (shown in stick representation) undergo conformational changes that accompany the change in redox state of the enzyme.

Asn110, respectively), these were omitted from the final model. The overall fold of ^{red}yGrx1 (Fig. 1*a*) is similar to those of the previously reported yGrx1 structures (PDB entries 3c1r, 3c1s and 2jac; Yu *et al.*, 2008; Håkansson & Winther, 2007), with four mixed β-strands in a central core structure surrounded by five α-helices.

The positions of the side chains (and in particular the thiol groups) of cysteine residues Cys27 and Cys30 were confirmed by the calculation of difference Fourier electron-density maps (using a model with the side chains of these residues removed; Fig. 1*b*). These residues were modelled with a distance between the S atoms of Cys27 and Cys30 of 3.2 Å, which is significantly greater than that observed (2.05 Å) for the ^{ox}yGrx1 structure (PDB entry 3c1r; Yu *et al.*, 2008). This indicates that the yGrx1 structure reported here is indeed that of ^{red}yGrx1 (PDB entry 6mws).

Superposition of the ^{red}yGrx1 structure with that of ^{ox}yGrx1 (PDB entry 3c1r; Yu *et al.*, 2008) gave a root-mean-square deviation (r.m.s.d.) of 0.48 Å for 108 common C$^{\alpha}$ positions, demonstrating that minimal conformational changes occur to the overall yGrx1 structure on oxidation and/or reduction. However, the reduction of the Cys27–Cys30 disulfide bond and separation of the thiol groups of these residues accompanies conformational rearrangements in the neighbouring protein structure, specifically residues Thr25, Tyr26 and His31 (Fig. 2). In the ^{ox}yGrx1 structure the side chain of Tyr26 faces 'away' from the Cys27–Cys30 site. In ^{red}yGrx1 Tyr26 shows a conformation rotated by approximately 180° from that observed for ^{ox}yGrx1, with the side chain orientated 'towards' the Cys27–Cys30 site. This is accompanied by a flip in the orientation of the carbonyl group of residue Thr25, so that in the ^{red}yGrx1 structure this group participates in a hydrogen-bonding interaction with the side chain of His31, which is also reorientated (Fig. 2). Interestingly, similar conformations for residues Thr25, Tyr26 and His31 were observed in the structure of ^{glu}yGrx1 (PDB entry 3c1s; Yu *et al.*, 2008), which also lacks a disulfide bond between residues Cys27 and Cys30 owing to the glutathionylation of Cys27. In addition, conformational changes of neighbouring amino acids have been reported for *E. coli* Grx1 (PDB entries 1ego and 1grx; Xia *et al.*, 1992) by NMR, in which reduction of the active-site Cys11–Cys14 disulfide bond was reported to result in an enhanced rate of exchange for the neighbouring residues Phe6, Gly7 and Ala17, indicating conformational changes in these residues.

In summary, although ^{red}yGrx1 crystallized in a different condition and space group to the reported ^{ox}yGrx1 and ^{glu}yGrx1 structures, the conformational changes of residues neighbouring the active site (CPYC), particularly Thr25, Tyr26 and His31, is consistent among the three structures. This indicates these changes are not owing to crystal packing and instead reflect the redox state of yGrx1. The precise role that these residues play in the activity of yGrx1 remains to be explored.

Acknowledgements

Aspects of this research were undertaken on the Macromolecular Crystallography beamline MX2 at the Australian Synchrotron, Victoria, Australia and we thank the beamline staff for their enthusiastic and professional support.

Funding information

This study was supported by ARC grant DP140102746 to MJM and an Australian Government Research Training Program Scholarship to SM.

References

Begas, P., Liedgens, L., Moseler, A., Meyer, A. J. & Deponte, M. (2017). *Nature Commun.* **8**, 14835.
Cave, J. W., Cho, H. S., Batchelder, A. M., Yokota, H., Kim, R. & Wemmer, D. E. (2001). *Protein Sci.* **10**, 384–396.
Chen, V. B., Arendall, W. B., Headd, J. J., Keedy, D. A., Immormino, R. M., Kapral, G. J., Murray, L. W., Richardson, J. S. & Richardson, D. C. (2010). *Acta Cryst.* D**66**, 12–21.
Emsley, P., Lohkamp, B., Scott, W. G. & Cowtan, K. (2010). *Acta Cryst.* D**66**, 486–501.
Evans, P. R. & Murshudov, G. N. (2013). *Acta Cryst.* D**69**, 1204–1214.
Håkansson, K. O. & Winther, J. R. (2007). *Acta Cryst.* D**63**, 288–294.
Holmgren, A. (1989). *J. Biol. Chem.* **264**, 13963–13966.
Kabsch, W. (2010). *Acta Cryst.* D**66**, 125–132.
Langer, G., Cohen, S. X., Lamzin, V. S. & Perrakis, A. (2008). *Nature Protoc.* **3**, 1171–1179.
Luikenhuis, S., Perrone, G., Dawes, I. W. & Grant, C. M. (1998). *Mol. Biol. Cell*, **9**, 1081–1091.
Martin, J. L. (1995). *Structure*, **3**, 245–250.
McCoy, A. J., Grosse-Kunstleve, R. W., Adams, P. D., Winn, M. D., Storoni, L. C. & Read, R. J. (2007). *J. Appl. Cryst.* **40**, 658–674.
Murshudov, G. N., Skubák, P., Lebedev, A. A., Pannu, N. S., Steiner, R. A., Nicholls, R. A., Winn, M. D., Long, F. & Vagin, A. A. (2011). *Acta Cryst.* D**67**, 355–367.
Prinz, W. A., Åslund, F., Holmgren, A. & Beckwith, J. (1997). *J. Biol. Chem.* **272**, 15661–15667.
Ritz, D. & Beckwith, J. (2001). *Annu. Rev. Microbiol.* **55**, 21–48.
Rodríguez-Manzaneque, M. T., Ros, J., Cabiscol, E., Sorribas, A. & Herrero, E. (1999). *Mol. Cell. Biol.* **19**, 8180–8190.
Ukuwela, A. A., Bush, A. I., Wedd, A. G. & Xiao, Z. (2017). *Biochem. J.* **474**, 3799–3815.
Ukuwela, A. A., Bush, A. I., Wedd, A. G. & Xiao, Z. (2018). *Chem. Sci.* **9**, 1173–1183.
Winn, M. D., Ballard, C. C., Cowtan, K. D., Dodson, E. J., Emsley, P., Evans, P. R., Keegan, R. M., Krissinel, E. B., Leslie, A. G. W., McCoy, A., McNicholas, S. J., Murshudov, G. N., Pannu, N. S., Potterton, E. A., Powell, H. R., Read, R. J., Vagin, A. & Wilson, K. S. (2011). *Acta Cryst.* D**67**, 235–242.
Xia, T.-H., Bushweller, J. H., Sodano, P., Billeter, M., Björnberg, O., Holmgren, A. & Wüthrich, K. (1992). *Protein Sci.* **1**, 310–321.
Yu, J., Zhang, N.-N., Yin, P.-D., Cui, P.-X. & Zhou, C.-Z. (2008). *Proteins*, **72**, 1077–1083.